PERGAMON

International Journal of Solids and Structures 37 (2000) 4083–4102

INTERNATIONAL JOURNAL OF SOLIDS and STRUCTURES

www.elsevier.com/locate/ijsolstr

Micromechanical modeling of transient waves from matrix cracking and fiber fracture in laminated beams

Mats Åberg*, Peter Gudmundson

Department of Solid Mechanics, Royal Institute of Technology, KTH 100 44, Stockholm, Sweden

Received 22 October 1998; in revised form 28 April 1999

Abstract

A micromechanical model for excitation of waves resulting from fiber fracture and matrix cracking in laminated beams is presented. The source is described as a time dependent displacement discontinuity and the wave propagation in the beam is modeled by a higher-order beam theory. The equations of motion defined by the beam model are then formally solved by employing integral transforms. Asymptotically valid solutions are subsequently found using residue calculus and the stationary phase method. As an example, a $[90/0_2/90]$ beam with a width to thickness ratio of 10 is considered. The dispersion curves resulting from the beam theory and three-dimensional finite element computations are compared and a maximum frequency for applicability of the beam theory is determined. The time response from fiber fracture and transverse matrix cracking is presented. The applications of the results to the analysis of acoustic emission experiments are also discussed.

Keywords: Transient waves; Beam; Bar; Dispersion; Matrix crack; Fiber fracture; Acoustic emission

1. Introduction

Damage properties of laminated composites are often found by uniaxial testing, see for example Gorman and Ziola (1991), Prosser et al. (1995) and Adolfsson and Gudmundson (1999). Important processes which precede specimen failure are matrix cracking and fiber fracture. These damage processes emit stress waves which can be used for localization, identification and quantification of damage provided one has an understanding of the wave field that develops in the specimen. It is thus interesting to model the wave fields created by matrix cracks and fiber fractures in thin laminated beams or bar-like

* Corresponding author. Fax: +46-8-411-2418.
E-mail address: matsa@hallf.kth.se (M. Åberg).

0020-7683/00/$ - see front matter
PII: S0020-7683(99)00147-X

specimens (hereafter collected under the term beam). The modeling can be divided into two basic parts. The first part is concerned with modeling of the damage event, i.e. the source. The second part is wave propagation in the beam-like specimen.

If the damage may be viewed as a displacement discontinuity, Burridge and Knopoff (1964) have shown how it may be replaced by equivalent volume forces that cause an identical wave field in the body. If the source is highly localized, i.e. the size of the source is much smaller than typical dimensions of the body and the considered wavelength, then, the geometry of the source and the displacement discontinuity are often collected in a so-called moment tensor, see for example the work by Rice (1980). The concept of moment tensors has been used with success in studies of micro cracking in different materials among others by Chang and Sachse (1986), Landis and Shah (1993), Ohtsu (1995), Guo (1996) and Guo et al. (1996). If the conditions for using the moment tensor are not met, one has to use the volume force in its full form. Gudmundson (1998), for example, has used this to study the radiation from a growing crack in a plate. In the present work, matrix cracking will be modeled as a time-dependent volume force confined to a line, and fiber fracture as a time-dependent moment tensor. Once volume forces due to the sources are known, the wave propagation must be addressed.

Wave propagation in elastic waveguides is complicated by the large number of reflections from the boundaries, or looking at a larger length-scale, by the fact that wave propagation is dispersive. Ceranoglu and Pao (1981) have studied wave fields from point sources in homogeneous isotropic plates by using the Green's function of a force in an unbounded solid. The response at a certain point is calculated by superposing reflections from the boundaries that reach the observation point. Because the number of reflections increase drastically with distance from the source, it is in practice only possible to consider points close to the source using this method. Vasudevan and Mal (1985) have also looked at wave fields from point sources in homogeneous isotropic plates. Integral transforms and numerical inversion are used and results for larger source-receiver distances are presented. Mal and Lih (1992) have studied dissipative unidirectional composite plates. Integral transforms in the in-plane variables and time are also used in that work. The transformed solution, which is a function of transform variables and the thickness coordinate, is inverted numerically. Laminated plates subjected to line loads have been considered by Green (1995). Integral transforms are used and the inversion is done numerically. Results for fairly large distances between load line and receiving point are presented.

A common feature in the investigations mentioned above is that the thickness coordinate in the plate appears explicitly. But, if the in-plane distances are much larger than the thickness of the plate, a homogenization in the thickness variable can be performed, i.e. a plate theory may be used. Lih and Mal (1995) have compared wave fields resulting from the use of a first-order transverse shear deformation plate theory due to Whitney and Pagano (1970) with the three-dimensional solution, and their conclusion is that good results can be achieved for large source-receiver distances and low frequencies.

Guo (1996) has used the first-order transverse shear deformation plate theory to study the flexural waves from matrix cracking, fiber fracture and other types of damage. Integral transforms are used in this work, but instead of using numerical inversion, residue-calculus and the stationary phase method are used to get an approximate spectrum, which is inverted to a time-signal by the use of FFT. The same kind of analysis and a theory for extension of plates, which takes lateral contraction into account, is used to study the extensional wave.

Flexural wave propagation in beams can be modeled using the Timoshenko beam theory. This is effectively the same as Whitney's plate theory if only wave propagation in one direction is considered, and instead of plane-strain stiffnesses, plane-stress stiffnesses perpendicular to that direction of propagation is used. Thus, the width of the beam never enters explicitly in the equations of motion and the range of validity, in frequency or wavelength, of the equations is uncertain.

Extension waves in bars with a homogeneous rectangular cross-section have been investigated by

Medick (1968). The displacement, stress and strain fields are expanded in Legendre polynomials with coefficients depending on the coordinate along the bar and time. A variation principle and truncation of the series are then used to generate a set of equations of motion, compatibility equations and constitutive relations as well as boundary and initial conditions. Muller and Touratier (1981) use a similar approach but allow for transversely isotropic materials. In both cases dispersion curves are presented and adjustment parameters (or correction factors) are introduced to fit certain points on the dispersion curves to known exact values.

Propagation of axially symmetric waves in semi-infinite laminated cylinders due to a tone burst at the end has been studied by Kohl et al. (1992). The displacements are expressed in frequency domain by a modal sum, and a tailor-made finite element code is used to compute the modal forms at a given frequency. The inversion to time domain is done using FFT.

In the present work, approximate equations of motion for symmetric cross-ply laminated composite uniaxial test specimens are derived using Hamilton's principle and assumed cross-section displacement fields. The equations of motion are then solved by Fourier transformation and approximate inversion using residue calculus and the stationary phase method.

2. Modeling of the sources

A laminate and a Cartesian coordinate system according to Fig. 1 is considered. The laminate is made of transversely isotropic plies. It is infinite in the 1-direction and bounded by free surfaces at $x_2 = \pm b$ and $x_3 = \pm h$. In modeling the sources, it is for simplicity assumed that the damage occurs in plies with the symmetry directions along the 1- or 2-direction, respectively (0°- and 90°-plies).

2.1. Matrix cracking

If the laminate under consideration is strained in the 1-direction, the first damage that typically appears is matrix cracking in the 90°-layers. It is often, if not always, found that the cracks will initiate at one of the edges and then propagate across the width of the specimen or stop within it, Prosser et al. (1995).

Consider a matrix crack at $x_1 = 0$ growing in the 2-direction. In the proceeding analysis, only wavelengths much larger than the ply thickness will be considered. For a dynamically growing matrix

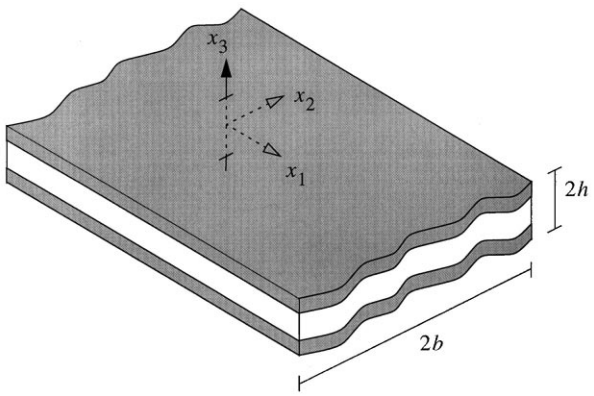

Fig. 1. Definition of the coordinate system used and geometry of the laminated beam.

crack, it can be assumed that a steady state crack opening will develop at a distance of the order of a few ply thicknesses behind the crack tip. Thus, if short wavelength information in the solution is ignored, the crack-opening displacement in the 1-direction may be expressed as

$$\Delta u_1(x_2, x_3, t) = \Delta u^{\text{stat}}(x_3) J_{\text{m}}(x_2, t), \tag{1}$$

where Δu^{stat} is the static crack-opening displacement of a crack in a laminate of infinite width subjected to the same strain in the 1-direction and to generalized plane strain in the 2-direction. The function J_{m} may within the same order of long wavelength approximation be expressed as

$$J_{\text{m}}(x_2, t) = \begin{cases} 0 & t < 0 \\ H(-x_2 - b + vt) & 0 \le t < 2b/v \\ 1 & 2b/v \le t \end{cases}, \tag{2}$$

where H is the Heaviside step-function. On a global scale it is a reasonable model of a crack growing across the entire width of the laminate with an average velocity, v. The crack-opening displacement may alternatively be viewed as a displacement discontinuity in the 1-direction. Using the work by Burridge and Knopoff (1964), it can be expressed by equivalent volume forces, f_i. The result in this case is

$$f_i = -C^{\text{T}}_{11ij} \frac{\partial}{\partial x_j} [J_{\text{m}}(x_2, t) \Delta u^{\text{stat}}(x_3) \delta(x_1)], \tag{3}$$

where δ is the Dirac delta-function and C^{T}_{ijkl} is the stiffness tensor of the 90°-ply containing the crack. The function Δu^{stat} has to be known in order to evaluate the expression in Eq. (3). One possible method is to perform finite element computations on a two-dimensional plane-strain model representing the cracked laminate and then fit a polynomial to the resulting crack-opening. Here an alternative method will be used.

Gudmundson and Zang (1993) have proposed a method to compute the stiffness-loss of a composite laminate containing matrix cracks. This is based on the assumption that the crack opening is mainly influenced by the state in the cracked ply, and that the rest of the plies have negligible direct influence on the crack-opening. This method has been found to yield very good stiffness-loss estimations, Adolfsson and Gudmundson (1995). With this in mind, the opening of an internal matrix crack can be approximated using the opening of a crack in an infinite plate under plane-strain, and the opening of a surface crack can be approximated by the opening of an edge crack in a semi-infinite plate under plane-strain. Expressions for these crack-openings may be found in the book by Wu and Carlsson (1991). Please note that, within the scope of the approximation, the anisotropy of the plies presents no problem since the material is isotropic in the plane of the crack. Once Δu^{stat} is known, the volume forces according to Eq. (3) can be calculated.

2.2. Fiber fracture

Further straining of the specimen will among other types of damage cause fiber fracture. Whereas matrix cracking is hardly localized to a point in uniaxial test, fiber fracture approximately is. Here a fiber fracture located at $x_1 = 0$, $x_2 = b_{\text{f}}$ and $x_3 = h_{\text{f}}$ within a 0°-ply is considered. The volume force can in this case be expressed in terms of a moment of tensor as

$$f_i = -M_{ij}(t) \frac{\partial}{\partial x_j} [\delta(x_1) \delta(x_2 - b_{\text{f}}) \delta(x_3 - h_{\text{f}})]. \tag{4}$$

The moment tensor, M_{ij}, is given by

$$M_{ij}(t) = \bar{u}^{\text{stat}} J_{\text{f}}(t) r^2 \pi C^{\text{f}}_{ij11}, \tag{5}$$

where $\bar{u}^{\text{stat}}$ is the average separation between the broken fiber ends under static loading, C^{f}_{ijkl} the stiffness tensor of the fiber and r the radius of the fiber. The time dependence is assumed to have the form

$$J_{\text{f}}(t) = \begin{cases} t/\tau & 0 < t < \tau \\ 1 & \tau < t \end{cases}. \tag{6}$$

This means that the average separation increases linearly during a time period of length τ to the value it would have in the static case.

The value of $\bar{u}^{\text{stat}}$ can be estimated in different ways. One possibility is to make an axisymmetric finite element model of the fiber and the surrounding matrix imbedded in a material having the material properties of the ply. Another possibility is to use the work of Case and Reifsnider (1996). In that case an integral equation has to be solved numerically.

Here, the simpler estimate due to Cox will be used, see Gibson (1994). Using Cox's model and letting the fiber length approach infinity, the separation of the fiber ends becomes

$$\bar{u}^{\text{stat}} = \bar{\epsilon}_1 r \sqrt{\frac{E_{\text{f}} \ \ln(1/V_{\text{f}})}{G_{\text{m}}}}, \tag{7}$$

where $\bar{\epsilon}_1$ is the strain in the 1-direction of the ply, r the radius of the fiber, E_{f} the elastic modulus of the fiber, V_{f} the fiber volume fraction and G_{m} the shear modulus of the matrix material.

3. Laminated beam models

Eqs. (3) and (4) define the sources considered in this work. Now wave propagation in the beam has to be addressed. The propagation of waves in laminated beam-like structures are complicated by reflections from boundaries. For wavelengths and distances larger than the dimensions of the cross-section, however, a beam model can often be used with success.

Consider a laminated beam loaded by volume forces f_i. In order to derive a beam model, i.e. to homogenize over the 2- and 3-directions, the displacements, u_i, are expressed in terms of Legendre polynomials,

$$u_i(x_j, t) = \sum_{n=0}^{\infty} \sum_{m=0}^{\infty} P_n\left(\frac{x_2}{b}\right) P_m\left(\frac{x_3}{h}\right) u_i^{(n,\,m)}(x_1, t), \tag{9}$$

where P_n is the Legendre polynomial of degree n. The next step is to truncate the series and use Hamilton's principle to generate equations of motion. Reflections from the ends of the specimen will not be considered in this work, and therefore, boundary conditions for the functions $u_i^{(n,\,m)}$ are not presented.

To get more lucid and manageable equations only symmetric laminates will be considered. For symmetric laminates, only certain combinations of n and m will appear together because the motion will be symmetric or antisymmetric with respect to the 2- and 3-axes. Thus, there are four basic types of wave propagation. Extensional wave propagation is symmetric with respect to both the 2- and 3-axes. Bending around the 2-axis is antisymmetric with respect to that axis and symmetric with respect to the 3-axis, and vice-versa for bending around the 3-axis. Twisting, finally, is antisymmetric with respect to both axes. Twisting motion will not be treated here because the sources that are considered in the

examples excite twisting through warping of the cross-section only, and hence, the motion due to twisting will generally be small.

In truncation of the series (9), use will also be made of the fact that the present work is concerned with thin beams, that is beams for which the width $2b$ is much larger than the thickness $2h$. In thin beams the stress σ_{33} will be small, at least for long wavelengths, and therefore, terms in the series (9) that have to do with lateral contraction in the 3-direction are omitted. Instead it is assumed that the material in the beam is under at state of plane stress. Hence, ply p follows the constitutive relation

$$\begin{bmatrix} \sigma_{11}^p \\ \sigma_{22}^p \\ \sigma_{23}^p \\ \sigma_{13}^p \\ \sigma_{12}^p \end{bmatrix} = \begin{bmatrix} c_{11}^p & c_{12}^p & 0 & 0 & c_{16}^p \\ c_{12}^p & c_{22}^p & 0 & 0 & c_{26}^p \\ 0 & 0 & c_{44}^p & c_{45}^p & 0 \\ 0 & 0 & c_{45}^p & c_{55}^p & 0 \\ c_{16}^p & c_{26}^p & 0 & 0 & c_{66}^p \end{bmatrix} \begin{bmatrix} \epsilon_{11}^p \\ \epsilon_{22}^p \\ \epsilon_{23}^p \\ \epsilon_{13}^p \\ \epsilon_{12}^p \end{bmatrix}, \tag{10}$$

where the ply stiffnesses c_{ij}^p are related to the stiffness tensor components for the ply, C_{ijkl}^p, in the following manner

$$c_{11}^p = C^p_{1111} - \frac{(C^p_{1133})^2}{C^p_{3333}}, \quad c_{12}^p = C^p_{1122} - \frac{C^p_{1133}C^p_{2233}}{C^p_{3333}}, \quad c_{22}^p = C^p_{2222} - \frac{(C^p_{2233})^2}{C^p_{3333}}$$

$$c_{16}^p = C^p_{1112}, \quad c_{26}^p = C^p_{2212}, \quad c_{44}^p = C^p_{2323}$$

$$c_{45}^p = C^p_{2313}, \quad c_{55}^p = C^p_{1313}, \quad c_{66}^p = C^p_{1212}. \tag{11}$$

In order to decide which terms to keep in Eq. (9), finite element computations were performed. This was done using the standard finite element code ABAQUS and a method for computing dispersion relations described in an earlier work, Åberg and Gudmundson (1997). The finite element computations give information about the dispersion relations and the corresponding wave forms. From the wave form of the highest considered mode at relatively long wavelengths it is possible to decide which terms to keep in the displacement expansion. In the present work, the two lowest modes will be modeled for each type of wave propagation. Doing finite element computations to get wave forms requires the geometry and materials to be specified. A width to thickness ratio of $b/h = 10$ was chosen and different material combinations were investigated. Changing the width to thickness ratio drastically and possibly also material properties will certainly change the conclusions, but a general treatment of this topic is beyond the scope of the present work. It is believed that the chosen displacement assumptions can be justified for other width to thickness ratios fairly close to 10.

Before proceeding to the detailed analysis, the following notation is introduced. Integrals over the thickness of the piecewise constant stiffness $c_{ij}(x_3)$ and density $\rho(x_3)$ are given the notation

$$[A_{ij}, D_{ij}] = \int_{-h}^{h} c_{ij}(x_3)[1, x_3^2]\mathrm{d}x_3 \tag{12}$$

and

$$[P, I] = \int_{-h}^{h} \rho(x_3)[1, x_3^2]\mathrm{d}x_3. \tag{13}$$

The generalized beam forces resulting from Hamilton's principle are written as

$$F_i^{(n,\,m)}(x_1,\,t)=\int_{-h}^{h}\int_{-b}^{b} f_i(x_j,\,t)P_n\left(\frac{x_2}{b}\right)P_m\left(\frac{x_3}{h}\right)\mathrm{d}x_2\,\mathrm{d}x_3. \tag{14}$$

3.1. Longitudinal motion

Based on the finite element computations the terms containing $u_1^{(0,0)}$, $u_1^{(2,0)}$ and $u_2^{(1,0)}$ are kept in the expansion. Hamilton's principle and Eqs. (10)–(14) lead to the following equations of motion

$$\begin{aligned}
&2A_{11}bu_{1,\,11}^{(0,\,0)}+2\eta A_{12}u_{2,\,1}^{(1,\,0)}+F_1^{(0,\,0)}=2Pb\ddot{u}_1^{(0,\,0)}\\
&-2\eta A_{12}u_{1,\,1}^{(0,\,0)}+\tfrac{2}{3}A_{66}bu_{2,\,11}^{(1,\,0)}-2\eta^2A_{22}b^{-1}u_2^{(1,\,0)}+2A_{66}u_{1,\,1}^{(2,\,0)}+F_2^{(1,\,0)}=\tfrac{2}{3}Pb\ddot{u}_2^{(1,\,0)}\\
&-2A_{66}u_{2,\,1}^{(1,\,0)}+\tfrac{2}{5}A_{11}bu_{1,\,11}^{(2,\,0)}-6A_{66}b^{-1}u_1^{(2,\,0)}+F_1^{(2,\,0)}=\tfrac{2}{5}Pb\ddot{u}_1^{(2,\,0)}
\end{aligned} \tag{15}$$

where the subscript ,1 and dot denotes derivation with respect to x_1 and time, respectively. In order to get a closer fit to the dispersion curve from the finite element computations a correction factor is introduced, similar to the work by Medick (1968) and Muller and Touratier (1981). The strain ϵ_{22} resulting from the assumed displacements is replaced by $\eta\epsilon_{22}$, and the factor η is then adjusted to achieve the best possible fit. The reason for choosing to correct the strain ϵ_{22} is that it was found to have the desired effect on the dispersion curves. See Section 5 for details regarding the correction factor.

3.2. Bending around the 2-axis

The finite element analyses showed that the terms containing $u_1^{(0,1)}$, $u_1^{(2,1)}$, $u_2^{(1,1)}$, $u_3^{(0,0)}$ and $u_3^{(2,0)}$ should be included to model the two lowest modes of wave propagation with sufficient accuracy in this case. The equations of motion resulting from Hamilton's principle are

$$\begin{aligned}
&2D_{11}\frac{b}{h^2}u_{1,\,11}^{(0,\,1)}-2A_{55}\frac{b}{h^2}u_1^{(0,\,1)}-2A_{55}\frac{b}{h}u_{3,\,1}^{(0,\,0)}+2\frac{\mu D_{12}}{h^2}u_{2,\,1}^{(1,\,1)}+F_1^{(0,\,1)}=2I\frac{b}{h^2}\ddot{u}_1^{(0,\,1)}\\
&2A_{55}\frac{b}{h}u_{1,\,1}^{(0,\,1)}+2A_{55}bu_{3,\,11}^{(0,\,0)}+F_3^{(0,\,0)}=2Pb\ddot{u}_3^{(0,\,0)}-2\frac{\mu D_{12}}{h^2}u_{1,\,1}^{(0,\,1)}\\
&-\frac{2}{3}D_{66}\frac{b}{h^2}u_{2,\,11}^{(1,\,1)}-\left(\frac{2\mu^2D_{22}}{bh^2}+\frac{2A_{44}b}{3h^2}\right)u_2^{(1,\,1)}+2\frac{D_{66}}{h^2}u_{1,\,1}^{(2,\,1)}\\
&-2\frac{A_{44}}{h}u_3^{(2,\,0)}+F_2^{(1,\,1)}=\frac{2Ib}{3h^2}\ddot{u}_2^{(1,\,1)}-2\frac{D_{66}}{h^2}u_{2,\,1}^{(1,\,1)}+\frac{2}{5}D_{11}\frac{b}{h^2}u_{1,\,11}^{(2,\,1)}\\
&-\left(\frac{6D_{66}}{bh^2}+\frac{2A_{55}b}{5h^2}\right)u_1^{(2,\,1)}-\frac{2}{5}A_{55}\frac{b}{h}u_{3,\,1}^{(2,\,0)}+F_1^{(2,\,1)}=\frac{2Ib}{5h^2}\ddot{u}_1^{(2,\,1)}\\
&-2\frac{A_{44}}{h}u_2^{(1,\,1)}+\frac{2}{5}A_{55}\frac{b}{h}u_{1,\,1}^{(2,\,1)}+\frac{2}{5}A_{55}bu_{3,\,11}^{(2,\,0)}-6\frac{A_{44}}{b}u_3^{(2,\,0)}+F_3^{(2,\,0)}=\frac{2}{5}Pb\ddot{u}_3^{(2,\,0)}.
\end{aligned} \tag{16}$$

In Eqs. (16) a correction factor, μ, has been introduced for the strain ϵ_{22} in the same manner as in Section 3.1. See Section 5 for details regarding μ.

3.3. Bending around the 3-axis

Based on the finite element computations the terms containing $u_1^{(1,0)}$, $u_1^{(3,0)}$, $u_2^{(0,0)}$ and $u_2^{(2,0)}$ are used to model the two lowest modes of wave propagation involving bending around the 3-axis. The resulting

equations of motion are

$$\begin{aligned}
&\frac{2}{3}A_{11}bu^{(1,\,0)}_{1,\,11} - 2\frac{A_{66}}{b}u^{(1,\,0)}_{1} - 2\frac{A_{66}}{b}u^{(3,\,0)}_{1} - 2A_{66}u^{(0,\,0)}_{2,\,1} + 2A_{12}u^{(2,\,0)}_{2,\,1} + F^{(1,\,0)}_{1} = \frac{2}{3}Pb\ddot{u}^{(1,\,0)}_{1}\\
&\quad - 2\frac{A_{66}}{b}u^{(1,\,0)}_{1} + \frac{2}{7}A_{11}bu^{(3,\,0)}_{1,\,11} - 12\frac{A_{66}}{b}u^{(3,\,0)}_{1} - 2A_{66}u^{(0,\,0)}_{2,\,1} - 2A_{66}u^{(2,\,0)}_{2,\,1} + F^{(3,\,0)}_{1} = \frac{2}{7}Pb\ddot{u}^{(3,\,0)}_{1}\\
&-2A_{66}u^{(1,\,0)}_{1,\,1} + 2A_{66}u^{(3,\,0)}_{1,\,1} + 2A_{66}bu^{(0,\,0)}_{2,\,11} + F^{(0,\,0)}_{2} = 2Pb\ddot{u}^{(0,\,0)}_{2}\\
&\quad - 2A_{12}u^{(1,\,0)}_{1,\,1} + 2A_{66}u^{(3,\,0)}_{1,\,1} + \frac{2}{5}A_{66}bu^{(2,\,0)}_{2,\,11} - 6\frac{A_{22}}{b}u^{(2,\,0)}_{2} + F^{(2,\,0)}_{2} = \frac{2}{5}Pb\ddot{u}^{(2,\,0)}_{2}.
\end{aligned} \tag{17}$$

For this type of motion no correction factors are introduced.

4. Asymptotic solution

The equations of motion are solved using Fourier transforms in time and length coordinates. The formal solution is approximately inverted using residue calculus and the stationary phase method.

4.1. Fourier transform

The following transform pairs for space and time, with transform variables ξ and ω, are applied to the equations of motion (15)–(17) (the subscript in x_1 will be dropped for convenience)

$$\hat{g}(\xi,\,t) = \int_{-\infty}^{\infty} g(x,\,t)\mathrm{e}^{-i\xi x}\,\mathrm{d}x, \quad g(x,\,t) = \frac{1}{2\pi}\int_{-\infty}^{\infty} \hat{g}(\xi,\,t)\mathrm{e}^{i\xi x}\,\mathrm{d}\xi, \tag{18}$$

$$g^{*}(x,\,\omega) = \int_{-\infty}^{\infty} g(x,\,t)\mathrm{e}^{i\omega t}\,\mathrm{d}t, \quad g(x,\,t) = \frac{1}{2\pi}\int_{-\infty}^{\infty} g^{*}(x,\,\omega)\mathrm{e}^{-i\omega t}\,\mathrm{d}\omega. \tag{19}$$

The resulting algebraic equations can be summarized using a matrix, $\mathbf{K}$, containing the stiffnesses A_{ij} and D_{ij}, a matrix, $\mathbf{M}$, containing the inertia factors P and I, the vector $\hat{\mathbf{f}}^{*}$, which has the transformed generalized beam forces $\hat{F}^{*(n,\,m)}_{i}$ as its elements and the vector $\hat{\mathbf{u}}^{*}$ containing the transformed displacement $\hat{u}^{*(n,\,m)}_{i}$. The result is

$$[\mathbf{K}(\xi) - \omega^{2}\mathbf{M}]\hat{\mathbf{u}}^{*} = \hat{\mathbf{f}}^{*}(\xi,\,\omega). \tag{20}$$

The homogeneous version of (20) defines an eigenvalue problem, and since the matrices $\mathbf{K}$ and $\mathbf{M}$ are Hermitian, it has p real eigenvalues, ω^{2}_{n}, and generally complex eigenvectors, $\mathbf{v}_{n}$. The eigenvectors are normalized such that

$$\mathbf{v}^{\mathrm{H}}_{n}\mathbf{K}\mathbf{v}_{n} = \omega^{2}_{n}, \tag{21}$$

$$\mathbf{v}^{\mathrm{H}}_{n}\mathbf{M}\mathbf{v}_{m} = \delta_{mn}, \tag{22}$$

where δ_{mn} is Kronecker's delta and the superscript 'H' denotes transpose and complex conjugation. Using relations (21) and (22) and Eq. (20) the transformed solution $\hat{\mathbf{u}}^{*}$ can be written as

$$\hat{\mathbf{u}}^*(\xi, \omega) = \sum_{n=1}^{p} \frac{\mathbf{v}_n^{\mathrm{H}}(\xi)\hat{\mathbf{f}}^*(\xi, \omega)}{\omega_n^2(\xi) - \omega^2}\mathbf{v}_n(\xi). \tag{23}$$

To get the time response at a certain position this expression has to be inverted using Eqs. (18) and (19).

4.2. Approximate inversion

The inversion of (23) is done approximately. First, it is inverted with respect to ξ,

$$\mathbf{u}^*(x, \omega) = \frac{1}{2\pi}\sum_{n=1}^{p}\int_{-\infty}^{\infty} \frac{\mathbf{v}_n^{\mathrm{H}}(\xi)\hat{\mathbf{f}}^*(\xi, \omega)}{\omega_n^2(\xi) - \omega^2}\mathbf{v}_n(\xi)\mathrm{e}^{i\xi x}\,\mathrm{d}\xi. \tag{24}$$

For $x > 0$, the integral may be evaluated in the complex plane by completing the integration path along the real-axis with a semi-circle of infinite radius in the complex plane, $\mathrm{Im}(\xi) > 0$. The integral along the infinite semi-circle will vanish, so (24) can be evaluated from residues of the poles, ξ_k, of the integrand in the upper complex plane. There will be poles with a non-vanishing imaginary part, but for large x their contribution will be negligible compared to the contribution from poles on the real-axis. Furthermore, for $x > 0$ only poles with positive group velocity give a contribution. Thus (24) can be approximated by

$$\mathbf{u}^*(x, \omega) = i\sum_{n=1}^{p}\sum_{k} \frac{\mathbf{v}_n^{\mathrm{H}}(\xi_k^n)\hat{\mathbf{f}}^*(\xi_k^n, \omega)}{2\omega_n(\xi_k^n)c_{gn}(\xi_k^n)}\mathbf{v}_n(\xi_k^n)\mathrm{e}^{i\xi_k^n x}, \tag{25}$$

where for a given mode n and value of ω, the value, ξ_k^n, is the kth ξ that satisfies all the following conditions

$$\mathrm{Im}(\xi) = 0, \quad \omega_n(\xi) = \pm\omega, \quad c_{gn}(\xi) > 0. \tag{26}$$

The group velocity, c_{gn}, of mode n is given as

$$c_{gn} = \frac{\mathrm{d}\omega_n}{\mathrm{d}\xi}. \tag{27}$$

It should be observed that there are combinations of ω and n for which no value of ξ satisfies the conditions given by (26). In that case the contribution to the spectrum will be zero.

The Fourier inversion with respect to ω of the spectrum (25) is formally defined from Eq. (19)

$$\mathbf{u}(x, t) = \frac{i}{2\pi}\sum_{n=1}^{p}\sum_{k}\int_{-\infty}^{\infty} \frac{\mathbf{v}_n^{\mathrm{H}}(\xi_k^n)\hat{\mathbf{f}}^*(\xi_k^n, \omega)}{2\omega_n(\xi_k^n)c_{gn}(\xi_k^n)}\mathbf{v}_n(\xi_k^n)\mathrm{e}^{it[\xi_k^n(x/t)-\omega]}\,\mathrm{d}\omega. \tag{28}$$

For the values of ω for which a ξ_k^n satisfying (26) exists, a variable transformation ($\omega \rightarrow \xi^n$) can be performed using the conditions in (26) and Eq. (27). The result of the transformation is

$$\mathbf{u}(x, t) = \frac{i}{2\pi}\sum_{n=1}^{p}\int_{\Gamma_n} \frac{\mathbf{v}_n^{\mathrm{H}}(\xi^n)\hat{\mathbf{f}}^*(\xi^n, \omega_n(\xi^n))}{2\omega_n(\xi^n)}\mathbf{v}_n(\xi^n)\mathrm{e}^{it[\xi^n(x/t)-\omega_n(\xi^n)]}\,\mathrm{d}\xi^n, \tag{29}$$

where Γ_n denotes the interval in ξ^n which satisfies the conditions in Eq. (26). Since the displacement vector $\mathbf{u}$ contains only real functions as its elements, the Fourier inversion in Eq. (28) may alternatively be expressed in terms of an integral for positive ω only. Hence, Eq. (29) may be rewritten as

$$\mathbf{u}(x,\,t) = -\frac{1}{2\pi}\mathrm{Im}\left[\sum_{n=1}^{p}\int_{\Gamma_n^+}\frac{\mathbf{v}_n^{\mathrm{H}}(\xi^{n+})\hat{\mathbf{f}}^*(\xi^{n+},\,\omega_n(\xi^{n+}))}{\omega_n(\xi^{n+})}\mathbf{v}_n(\xi^{n+})\mathrm{e}^{it[\xi^{n+}(x/t)-\omega(\xi^{n+})]}\,\mathrm{d}\xi^{n+}\right], \tag{30}$$

where Γ_n^+ is the subset of Γ_n including ξ^{n+} corresponding to $\omega > 0$. The expression for the velocities $\dot{\mathbf{u}}$ may now easily be determined from Eq. (30),

$$\dot{\mathbf{u}}(x,\,t) = \frac{1}{2\pi}\mathrm{Re}\left\{\sum_{n=1}^{p}\int_{-\infty}^{\infty}[\mathbf{v}_n^{\mathrm{H}}(\xi^{n+})\hat{\mathbf{f}}^*(\xi^{n+},\,\omega_n(\xi^{n+}))]\mathbf{v}_n(\xi^{n+})\mathrm{e}^{it[\xi^{n+}(x/t)-\omega(\xi^{n+})]}\,\mathrm{d}\xi^{n+}\right\}. \tag{31}$$

If large values of t are considered the integrals in (30) or (31) can be asymptotically expanded using the stationary phase method, see Borovikov (1994). The leading term of the expansion of Eq. (31) is

$$\dot{\mathbf{u}}(x,\,t) = \frac{1}{2\sqrt{\pi}}\mathrm{Re}\left\{\sum_{n=1}^{P}\sum_{j}\sqrt{\frac{1}{\mid\omega_{nj}''\mid t}}[1-\mathrm{sgn}(\omega_{nj}'')i][\mathbf{v}_{nj}^{\mathrm{H}}\hat{\mathbf{f}}_{nj}^*]\mathbf{v}_{nj}\,\mathrm{e}^{it[\xi_j^{n+}(x/t)-\omega_{nj}]}+O(t^{-3/2})\right\}, \tag{32}$$

where ξ_j^{n+} are the values of ξ^{n+} that for a given ratio x/t satisfy

$$c_{gn}(\xi^{n+}) = \frac{x}{t}. \tag{33}$$

The subscript nj signifies that the function should be evaluated at ξ_j^{n+}. If the group velocity is stationary, i.e. $\omega_n''=0$ (or equivalently when two different points ξ_j^{n+} and ξ_{j+1}^{n+} coincide), the expansion in (32) is no longer valid. Close to such points a refined expansion, which involves the Airy function and its derivative, has to be used. Details may be found in the book by Borovikov (1994), which also presents criteria for changing between the refined expansion and expression (32).

5. Examples

A symmetric cross-ply ([90/$0_2$90]) with ply properties given in Table 1 is considered. The width to thickness ration, b/h, is set to 10. Fig. 2 shows calculated dispersion curves for this laminate.

The squares correspond to values for bending around the 2-axis obtained by finite elements. The solid curves close to the squares are the two lowest dispersion curves (labeled B2-1 and B2-2) resulting from the equations of motion (16) with the correction factor $\mu=0.82$. The dashed curve close to the squares of the second mode shows the dispersion relation without a correction factor or in other words with $\mu=1$ (for the lowest mode the dashed curve and the solid curve are on top of each other). The triangles show finite element values for bending around the 3-axis. The solid curves close to the triangles are the two lowest dispersion curves (labeled B3-1 and B3-2) given by the equations of motion of Section 3.3, that is Eq. (17). Circles show finite element results for extensional motion. The curves close to the circles

Table 1
Properties of the glass fiber reinforced epoxy ply

E_{L} (GPa)	E_{T} (GPa)	ν_{LT}	ν_{TT}	G_{LT} (GPa)	ρ (kg/m^3)
46	18	0.29	0.42	7.9	1930

show the dispersion relations for the two lowest modes (the lowest labeled E) obtained from the equations of motion in (15). For the solid curves the values of the correction factor was $\eta = 0.87$, and the dashed curves show the dispersion curves for $\eta = 1$.

According to the finite element computations, the second optical modes (not shown) start at a value of about 2.6, 3.9 and 2.6 in the diagram for bending around the 2-axis, bending around the 3-axis and extension, respectively. Therefore, a maximum circular frequency

$$\omega_{\max} = 2.5\frac{\sqrt{E_L/\rho}}{2b}, \tag{34}$$

is used in the computations. This corresponds to adding a fourth condition to Eq. (26), namely

$$\omega_n(\xi) < \omega_{\max} . \tag{35}$$

Fig. 3 shows the dimensionless group velocity, $c_g\sqrt{\rho/E_L}$, versus dimensionless frequency according to the equations of motion derived in Section 3. The solid, long dashed and short dashed curves correspond to extension (E), being around the 3-axis (B3-1 and B3-2) and bending around the 2-axis (B2-1 and B2-2), respectively. This diagram is helpful in analyzing the calculated time-responses.

5.1. Fiber fracture

The generalized beam-forces for the fiber fracture case are found by inserting the volume forces of Eq. (4) in the integral (14). The result is

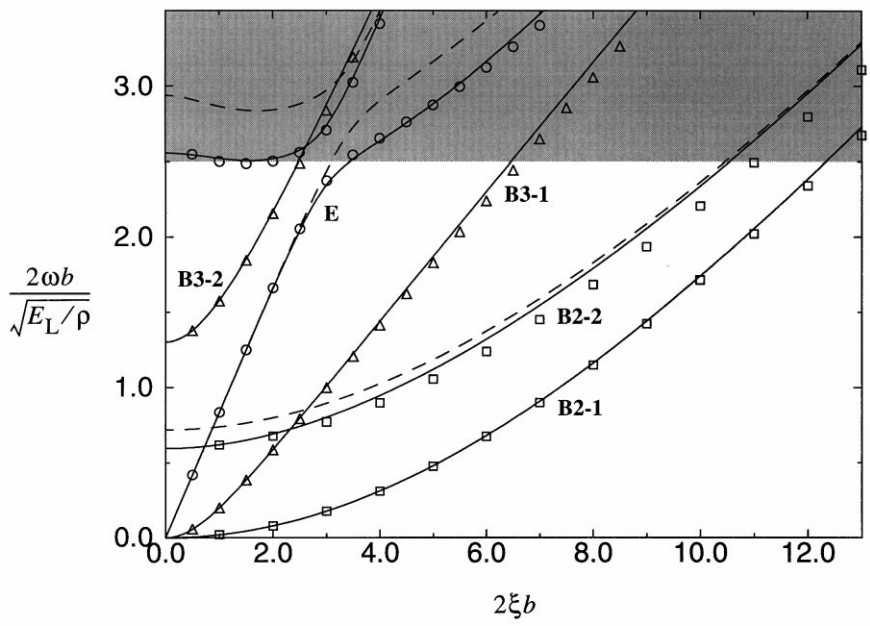

Fig. 2. Dimensionless frequency versus dimensionless wavenumber for a $[90/0_2/90]$ laminated beam with $b/h = 10$. The symbols are finite element results, and the curves result from the derived beam model with (solid) and without (dashed) correction factors. The shading marks the maximum frequency considered in Fourier inversion. The labels E, B2 and B3 mark the modes associated with extension and bending around the 2- and 3-axes, respectively.

$$F_1^{(n,\,m)} = -M_{11}(t)\delta'(x_1)P_n\left(\frac{b_f}{b}\right)P_m\left(\frac{h_f}{h}\right), \quad \begin{matrix} n = 0,\ \ldots,\ 3 \\ m = 0,\ 2 \end{matrix}$$

$$F_2^{(1,\,m)} = M_{22}(t)\frac{\delta(x_1)}{b}P_m\left(\frac{h_f}{h}\right), \quad m = 0,\ 1$$

$$F_2^{(2,\,0)} = M_{22}(t)\frac{3b_f\delta(x_1)}{b^2}$$

$$F_2^{(0,\,0)} = F_3^{(0,\,0)} = F_3^{(2,\,0)} = 0, \tag{36}$$

where prime denotes derivation. The assumed properties of the glass fibers and the epoxy matrix are given in Table 2. Using rule of mixtures, see for example Gibson (1994), and the known value of longitudinal modulus, E_L, or the density, ρ, the values of Table 2 give the fiber volume fraction, $V_f = 0.6$. The ratio between fiber diameter and width is set to a typical values $r/b = 5 \times 10^{-4}$. The position of the fiber fracture is set to $h_f = h/4$, $b_f = b/2$, and the strain, $\bar{\epsilon}_1$, is assumed to have the value 2%. It is also assumed that the fracture takes place during the time $\tau = 2r/\sqrt{E_f/\rho_f}$. Using the method described in Section 4 it is possible to calculate the velocity, $\dot{\mathbf{u}}$, as a function of time at a given position, x_i, for sufficiently large x_1. Figs. 4–6 show the velocities $\dot{u}_1$, $\dot{u}_2$ and $\dot{u}_3$, respectively, of the upper right corner ($x_2 = b$, $x_3 = h$) at $x_1 = 100b$ as a function of time. In Figs. 4 and 5 the labeled arrows mark the arrival of the different types and modes of wave propagation. Their arrival times are easily calculated

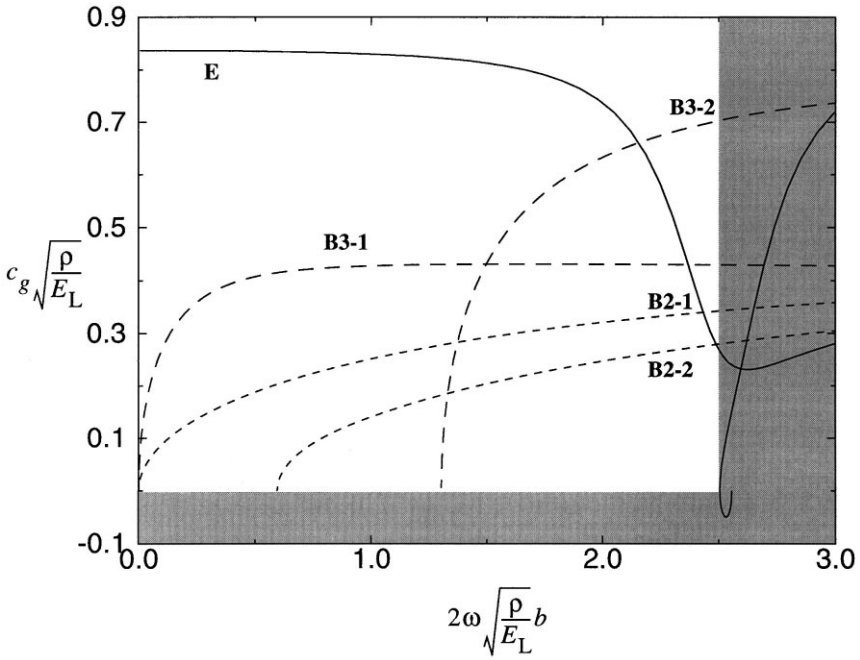

Fig. 3. Dimensionless group velocity versus dimensionless frequency for a $[90/0_2/90]$ laminated beam with $b/h = 10$. Curves for wave propagation associated with extension (solid), bending around the 3-axis (long dashed) and bending around the 2-axis (dashed) are shown.

Table 2
Properties of the glass fiber (f) and the epoxy matrix (m)

E_f (GPa)	ν_f	ρ_f (kg/m^3)	E_m (GPa)	ν_m	ρ_m (kg/m^3)
73	0.22	2492	4.0	0.35	1120

from the maximum group velocities of the modes, which can be read from the curves in Fig. 3. The extension and bending around the 3-axis do not contribute directly to the vertical velocity, $\dot{u}_3$, and therefore, only the arrival of the first and second modes of bending around the 2-axis are shown in Fig. 6.

5.2. Matrix cracking

In this section the generalized beam forces of Section 3 are derived for a transverse surface matrix crack in the top 90°-ply. The beam is assumed to be loaded to a strain $\bar{\epsilon}_1$ in the 1-direction. Disregarding edge effects, this strain gives the following stress in the 90°-plies.

$$\bar{\sigma}_1^{90^\circ} = \frac{E_L^2 E_T + (1 - 2\nu_{LT}^2) E_L E_T^2}{(E_L - E_T \nu_{LT}^2)(E_L + E_T)} \bar{\epsilon}_1. \tag{37}$$

The static crack opening displacement can be estimated using the fact that the beam is much wider than

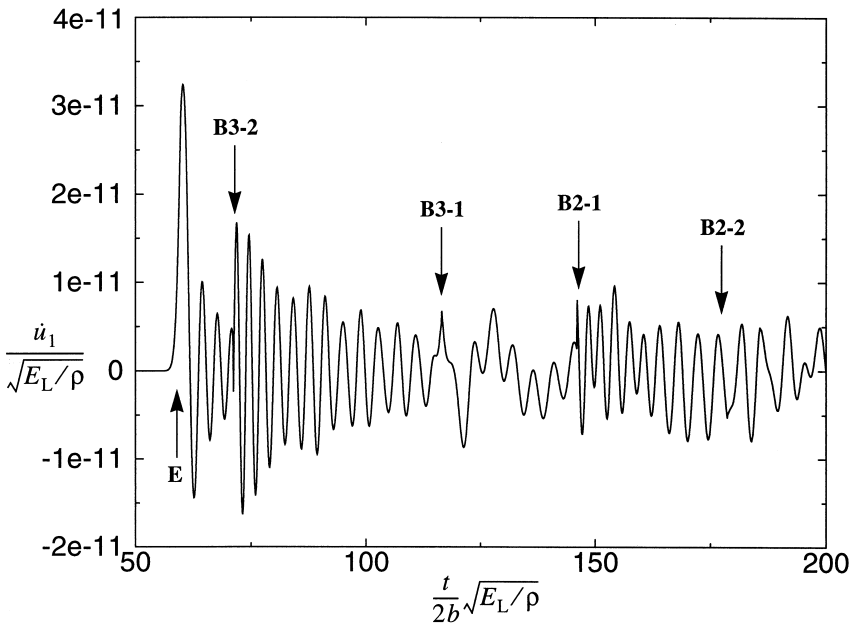

Fig. 4. Horizontal velocity in the 1-direction of the corner $x_2 = b$ and $x_3 = h$ at $x_1 = 100b$ due to fiber fracture. The labeled arrows mark the arrival of the extensional wave (E), the second and first modes of bending around the 3-axis (B3-2 and B3-1) and the first and second modes of bending around the 2-axis (B2-1 and B2-2).

it is thick. The crack is thus in a state of generalized plane strain. Referring back to the discussion in Section 2.1, the static crack opening of the surface crack is taken to be (Wu and Carlsson, 1991),

$$\Delta u^{\text{stat}}(\eta) = \frac{h}{\sqrt{2}} \frac{(1-\nu_{\text{TT}}^2)}{E_{\text{T}}} \bar{\sigma}_1^{90^\circ} \sqrt{\eta}(\alpha_1 + \alpha_2\eta + \alpha_3\eta^2 + \alpha_4\eta^3), \tag{38}$$

where the dimensionless coordinate η is defined by the relation

$$x_3 = \frac{h}{2}(\eta + 1), \tag{39}$$

and

$$\alpha_1 = 4.486, \quad \alpha_2 = -0.7635, \quad \alpha_3 = 0.3453, \quad \alpha_4 = 0.0456. \tag{40}$$

The insertion of (38) in (3), and subsequently in (14), gives the following generalized beam forces

$$F_1^{(n,\,0)} = -0.9878 C^{\text{T}}_{1111} \delta'(x_1)\gamma_n(t) h^2 \bar{\sigma}_1^{90^\circ} \frac{(1-\nu_{\text{TT}}^2)}{E_{\text{T}}}, \quad n = 0, \ldots, 3$$

$$F_1^{(m,\,1)} = -0.7876 C^{\text{T}}_{1111} \delta'(x_1)\gamma_0(t) h^2 \bar{\sigma}_1^{90^\circ} \frac{(1-\nu_{\text{TT}}^2)}{E_{\text{T}}}, \quad m = 0, 2$$

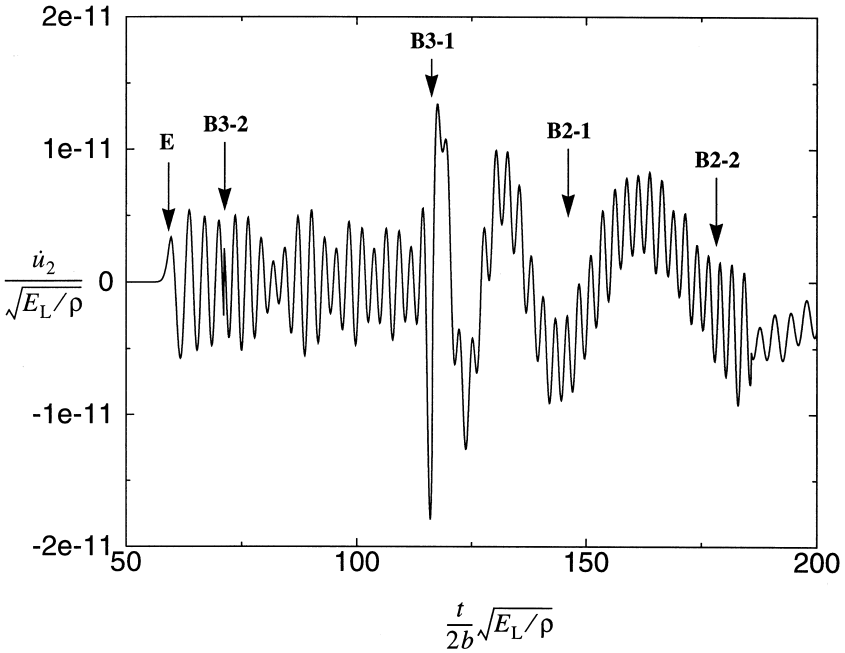

Fig. 5. Horizontal velocity in the 2-direction of the corner $x_2 = b$ and $x_3 = h$ at $z_1 = 100b$ due to fiber fracture. The labeled arrows mark the arrival of the extensional wave (E), the second and first modes of bending around the 3-axis (B3-2 and B3-1) and the first and second modes of bending around the 2-axis (B2-1 and B2-2).

$$F_2^{(n,\,0)} = 0.9878 C^{\mathrm{T}}_{1122}\delta(x_1)\gamma_{n-1}(t)(2n-1)\frac{h^2}{b}\bar{\sigma}_1^{90^\circ}\frac{(1-\nu_{\mathrm{TT}}^2)}{E_{\mathrm{T}}}, \quad n = 1, 2$$

$$F_2^{(1,\,1)} = 0.7876 C^{\mathrm{T}}_{1122}\delta(x_1)\gamma_0(t)\frac{h^2}{b}\bar{\sigma}_1^{90^\circ}\frac{(1-\nu_{\mathrm{TT}}^2)}{E_{\mathrm{T}}}; \quad F_2^{(0,\,0)} = 0$$

$$F_3^{(0,\,0)} = F_3^{(2,\,0)} = 0. \tag{41}$$

The prime denotes derivation and the functions γ are given by

$$\gamma_0(t) = \begin{cases} 0 & t < 0 \\ vt & 0 \le t \le 2b/v \\ 2b & t > 2b/v \end{cases}, \tag{42}$$

$$\gamma_1(t) = \begin{cases} 0 & t < 0 \\ (v^2t^2 - 2bvt)/(2b) & 0 \le t \le 2b/v \\ 0 & t > 2b/v \end{cases}, \tag{43}$$

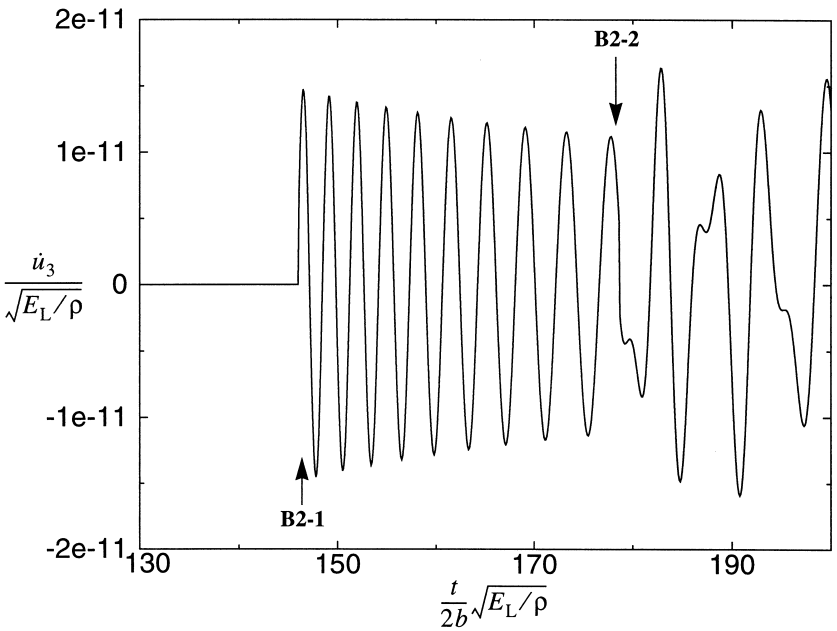

Fig. 6. Vertical velocity of the corner $x_2 = b$ and $x_3 = h$ at $x_1 = 100b$ due to fiber fracture. The labeled arrows mark the arrival of the first and second modes of bending around the 2-axis (B2-1 and B2-2).

$$\gamma_2(t) = \begin{cases} 0 & t < 0 \\ vt(v^2t^2 + 2b^2 - 3bvt)/2b^2 & 0 \le t \le 2b/v \\ 0 & t > 2b/v \end{cases}, \tag{44}$$

$$\gamma_3(t) = \begin{cases} 0 & t < 0 \\ \dfrac{5v^4t^4}{3b^3} - \dfrac{5v^3t^3}{2b^2} + \dfrac{3v^2t^2}{b} - vt & 0 \le t \le 2b/v \\ 0 & t > 2b/v \end{cases}. \tag{45}$$

The average velocity of the propagating surface crack, v, is set to $0.1\sqrt{E_L/\rho}$. For the material considered this translates to 488 m/s. The value of the strain, $\bar{\epsilon}_1$, is set of 0.6%, in accordance with experiments performed on the material by Adolfsson and Gudmundson (1999).

Figs. 7–9 show the velocities $\dot{u}_1$, $\dot{u}_2$, and $\dot{u}_3$, respectively, of the upper right corner of the beam ($x_2 = b$, $x_3 = h$) at $x_1 = 100b$ as function of time. In Figs. 7 and 8 the labeled arrows mark the arrival of the extension wave (E), the fast and slow waves associated with bending around the 3-axis (B3-2 and B3-1), the fast and slow waves associated with bending around the 2-axis (B2-1 and B2-2). The extensional and bending around the 3-axis waves do not contribute directly to the vertical speed, $\dot{u}_3$, and therefore, only the arrival of the fast and slow bending around the 2-axis waves are shown in Fig. 9.

Matrix cracking is a very slow event compared to fiber fracture. This means that the distance from the source to the observation point has to be approximately $x = 1000b$ for the stationary phase method

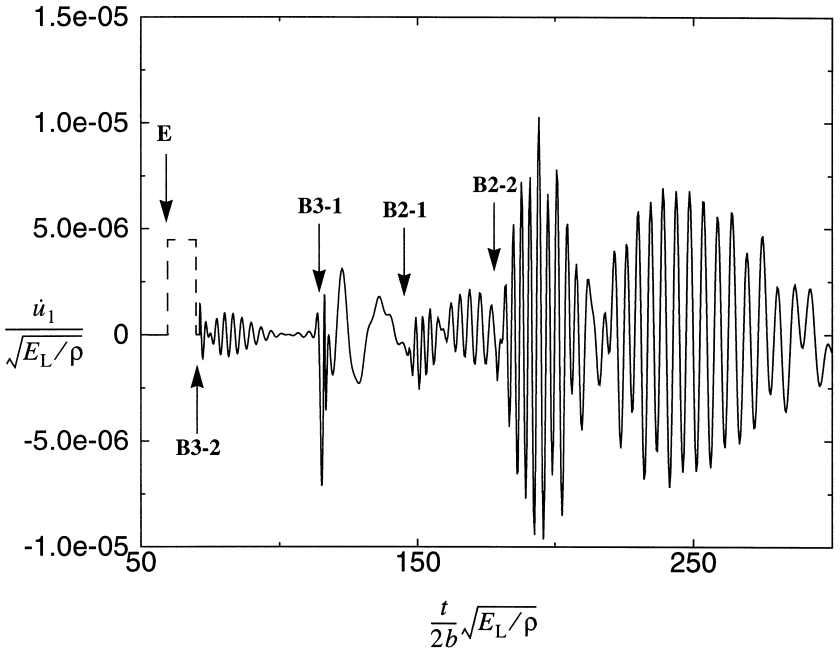

Fig. 7. Horizontal velocity in the 1-direction of the corner $x_2 = b$ and $x_3 = h$ at $x_1 = 100b$ due to matrix cracking. The labeled arrows mark the arrival of the extensional wave (E), the second and first modes of bending around the 3-axis (B3-2 and B3-1) and the first and second modes of bending around the 2-axis (B2-1 and B2-2). The ordinary wave equation was in this case used to compute the response from extensional motion (dashed).

to be accurate for the extensional wave in the case of matrix cracking. Therefore, the extensional motion is, in this case, modeled by assuming constant displacement of the cross-section in the 1-direction, plane strain in the 2-direction and plane stress in the 3-direction. This leads to the ordinary wave equation which does not exhibit dispersion. The resulting velocity in the 1-direction of the cross-section can be seen as the dashed square pulse in Fig. 7. This pulse has not been subjected to the filter described by Eq. (35). The simpler model does not give any explicit motion in the 2- and 3-directions and therefore, there is no response from extension motion in Figs. 8 and 9.

6. Discussion

The present modeling of transient wave motion resulting from fiber fracture and matrix cracking has two separate parts. The first part, which is independent of the second, is concerned with modeling of the sources. Questions could be raised regarding the specific time functions, J_f and J_m, used, but answers based on experiments are hard to provide because of the small time and length scales involved. More refined techniques for finding the static opening of the matrix crack and fractured fiber could also, as suggested, be used, but considering the level of approximation involved in the modeling of wave propagation and time dependence of the sources it is not crucial. In reality a damage event may also include combinations of the mechanisms modeled here. Fracture of a single fiber may for example initiate fracture of fibers around it resulting in a response with larger amplitude and longer duration. The model presented here is linear, so the total response from several events, or sources, can be obtained by superposition of the individual contributions.

Comparing the dispersion curves from finite element computations and the developed beam models,

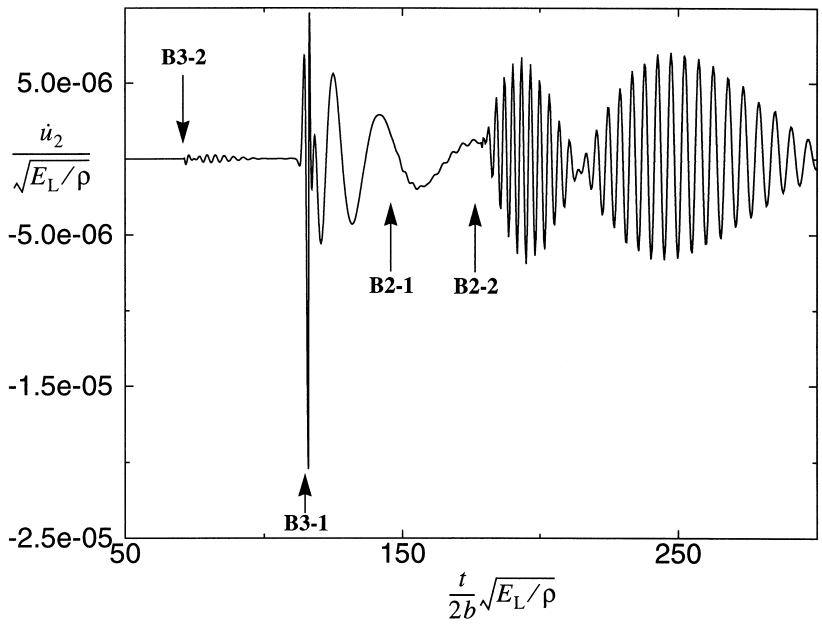

Fig. 8. Horizontal velocity in the 2-direction of the corner $x_2 = b$ and $x_3 = h$ at $x_1 = 100b$ due to matrix cracking. The labeled arrows mark the arrival of the second and first modes of bending around the 3-axis (B3-2 and B3-1) and the first and second modes of bending around the 2-axis (B2-1 and B2-2).

the use of the beam models for the considered example seems justifiable up to the circular frequency given by Eq. (34). For a typical specimen this translates to a frequency of 50 kHz. At this frequency, the model B2-1 has the shortest wavelength, and it is approximately half the beam width. The generalized beam forces derived show that many modes of wave propagation of appreciable amplitude are excited by fiber fracture and matrix cracking. The time dependence of the beam forces also show that matrix cracking, as modeled here, is a slow process compared to fiber fracture. The main parameter in the time-dependence is the time it takes for the damage to fully develop. That is $2b/v$ for the matrix crack and τ for the fiber fracture. This time governs how fast the Fourier transform decreases with respect to frequency, and frequencies higher than frequencies of the order of the inverse of this time will mainly influence the details of the growth behavior. It may, therefore, be argued that there is a mismatch in the modeling of the response from matrix cracking. The time dependence of the source can be modeled with confidence for frequencies lower than approximately $0.1(2b)^{-1}\sqrt{E_L/\rho}$, whereas the wave propagation is modeled up to a circular frequency of $2.5(2b)^{-1}\sqrt{E_L/\rho}$, thus in the case of matrix cracking a simpler beam model, as indicated in the last paragraph of Section 5, may be sufficient. This is not the case for fiber fracture because the relevant frequency in this case is approximately $200(2b)^{-1}\sqrt{E_l/\rho}$.

The method used to solve the equations of motion approximately, Fourier transforms and inversion by residue-calculus and the stationary phase method, is fast and involves very few numerical difficulties. The only complication being stationary values of the group velocity, c_g, which are found on the E and B3-1 mode curves (see Fig. 3). As discussed earlier, a refined version of the expansion in Eq. (32) has to be used for such points. A limitation of the inversion method used is that the time, or equivalently the distance from the source, has to be large.

The time response curves for fiber fracture (Figs. 4–6) show fairly even amplitudes. The discontinuities seen in the curves are due to the unphysical sharp 'filter' of Eq. (35). The relatively sharp

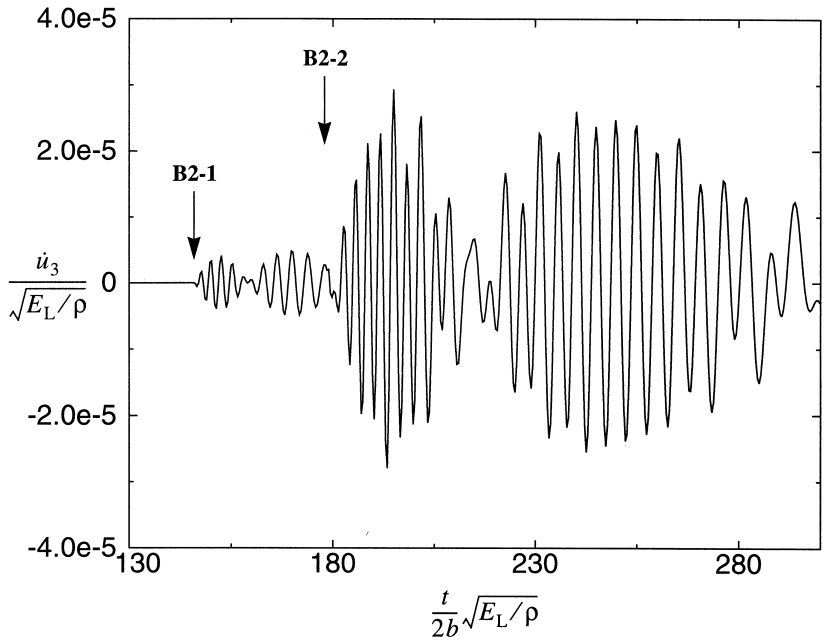

Fig. 9. Vertical velocity of the corner $x_2 = b$ and $x_3 = h$ at $x_1 = 100b$ due to matrix cracking. The labeled arrows mark the arrival of the first and second modes of bending around the 2-axis (B2-1 and B2-2).

peak at the beginning of the signal in Fig. 4 corresponds to the stationary group velocity of the extensional wave. In Fig. 5 there is a less pronounced peak corresponding to the stationary value of the group velocity in the dispersion relation of the B3-1 mode. The velocity of lateral contraction in the 2-direction is seen as a component of the signal in Fig. 5. Its amplitude is approximately constant and can be seen uninterfered until the B3-2 mode appears. The amplitude is close to 5×10^{-12} in the diagram. It is reasonable that lateral contraction velocity in the 3-direction is approximately 1/10 of that value, because of the ratio between height and width. Looking at the amplitude of the signal in Fig. 6 it seems justifiable to neglect the vertical velocity due to lateral contraction.

The amplitudes of the time response due to matrix cracking (Figs. 7–9) are roughly 5×10^{6} times larger than the amplitude from a single fiber fracture. The time response due to matrix cracking also show more variation in amplitude. In Fig. 8 a sharp peak in the amplitude corresponding to the stationary value of the group velocity in the B3-1 curve can be seen. The effect of dispersion is also evident in Fig. 8 for this mode at least until the arrival of the B2-2 mode interferes with the signal. The low frequencies travel slower for the B3-1 model.

Some of the results presented here can be useful in understanding acoustic emission experiments. For example, this work shows that many different modes of propagation are excited on the beam level by a damage event. Also, the relative amplitudes of the different modes and types of wave propagation can be estimated. There are however, complications if one wants to use the present method to predict time signals of an acoustic emission experiment. The inversion technique used requires distances from the source that normally are larger than the length of typical specimens. This could be alleviated by inverting Eq. (23) numerically. The maximum typical frequency modeled in this work is around 50 kHz which must be considered low compared to the frequencies recorded in experiments. A remedy could be to use a plate or three-dimensional model instead. Reflections from the ends of the specimen is also seen in acoustic emission experiments. A more complete model should also include that feature.

7. Conclusions

Based on the present work it is concluded that many different modes of propagation are excited by matrix cracking and fiber fracture in a thin laminated beam. Far away from the source, where it is reasonable to assume that the specimen behaves as a beam, matrix cracking is a low frequency event. Typically important frequencies are less than 10 kHz. Fiber fracture on the other hand is associated with high frequencies. The fit between dispersion relations from finite element analyses and the beam theory indicates that a laminated beam model can be used to model the behavior of the beam up to the frequency of the lowest mode not modeled in the assumed displacement field. Inverting the Fourier transformed equations of motion by residue–calculus and the method of stationary phase limits the applicability of the method presented.

Acknowledgements

Financial support from the Swedish Research Council for Engineering Sciences (TFR) is gratefully acknowledged.

References

Åberg, M., Gudmundson, P., 1997. The usage of standard finite element codes for computation of dispersion relations in materials with periodic microstructure. Journal of the Acoustical Society of America 102 (4), 2007–2013.

Adolfsson, E., Gudmundson, P., 1995. Matrix crack induced stiffness reductions in $[(0_m/90_m/+\theta_p/-\theta_q)_S]_M$ composite laminates. Composites Engineering 5, 107–123.

Adolfsson, E., Gudmundson, P., 1999. Matrix crack initiation and progression in composite laminates subjected to bending and extension. International Journal of Solids and Structures 36 (21), 3131–3169.

Borovikov, V.A., 1994. Uniform Stationary Phase Method. The Institution of Electrical Engineers, London, UK.

Burridge, R., Knopoff, L., 1964. Body force equivalents for seismic dislocations. Bulletin of the Seismological Society of America 54 (6), 1875–1888.

Case, S.W., Reifsnider, K.L., 1996. Micromechanical analysis of fiber fracture in unidirectional composite materials. International Journal of Solids and Structures 33 (26), 3795–3812.

Ceranoglu, A.N., Pao, Y-H., 1981. Propagation of elastic pulses and acoustic emission in a plate, Parts 1–3. Journal of Applied Mechanics 48, 125–147.

Chang, C., Sachse, W., 1986. Frequency division method for AE source characterization. Journal of the Acoustical Society of America 79 (5), 1307–1316.

Gibson, R.F., 1994. Principles of Composite Material Mechanics. McGraw-Hill, New York.

Gorman, M.R., Ziola, S.M., 1991. Plate waves produced by transverse matrix cracking. Ultrasonics 29, 245–251.

Green, E.R., 1995. Acoustic emission sources in a cross-ply laminated plate. Composites Engineering 5 (12), 1453–1469.

Gudmundson, P., 1998. On acoustic emissions and dynamic energy release rates for steady state growing tunneling cracks in laminated plates. Department of Solid Mechanics, KTH, Report 221, ISRN KTH/HFL/R-98/03-SE, TRITA HFL-221 ISSN 0281-1502.

Gudmundson, P., Zang, W., 1993. An analytical model for thermoelastic properties of composite laminates containing transverse matrix cracks. International Journal of Solids and Structures 30, 3211–3231.

Guo, D., 1996. Lamb waves from microfractures in composite plates. Ph.D. thesis, Mechanical Engineering, University of California, LA.

Guo, D., Mal, A., Ono, K., 1996. Wave theory of acoustic emission in composite laminates. Journal of Acoustic Emission 14, S19–S46.

Kohl, T., Datta, S.K., Shah, A.H., 1992. Axially symmetric pulse propagation in semi-infinite hollow cylinders. AIAA Journal 30 (6), 1617–1624.

Landis, E.N., Shah, S.P., 1993. Recovery of microcrack parameters in mortar using quantitative acoustic emission. Journal of Nondestructive Evaluation 12 (4), 219–232.

Lih, S-S., Mal, A.K., 1995. On the accuracy of approximate plate theories for wave field calculations in composite laminates. Wave Motion 21, 17–34.

Mal, A.K., Lih, S-S., 1992. Elastodynamic response of a unidirectional composite laminate to concentrated surface load: Parts I–II. Journal of Applied Mechanics 59, 878–892.

Medick, M.A., 1968. Extensional waves in elastic bars of rectangular cross section. Journal of the Acoustical Society of America 43, 152–161.

Muller, P., Touratier, M., 1981. Dispersion of longitudinal waves in a rectangular transversely isotropic wave-guide. Wave Motion 3, 181–202.

Ohtsu, M., 1995. Acoustic emission theory for moment tensor analysis. Res. Nondestr. Eval. 6, 169–184.

Prosser, W.H., Jackson, K.E., Kellas, S., Smith, B.T., McKeon, J., Friedman, A., 1995. Advanced waveform-based acoustic emission detection of matrix cracking in composites, Materials Evaluation 53, 1052–1058.

Rice, J.R., 1980. Elastic wave emission from damage processes. Journal of Nondestructive Evaluation 1 (4), 215–223.

Vasudevan, N., Mal, A.K., 1985. Response of an elastic plate to localized transient sources. Journal of Applied Mechanics 52, 356–362.

Whitney, J.M., Pagano, N.J., 1970. Shear deformation in heterogeneous anisotropic plates. Journal of Applied Mechanics 37, 1031–1036.

Wu, X-R., Carlsson, A.J., 1991. Weight Functions and Stress Intensity Factor Solutions. Pergamon, Oxford, UK.